Measuring Ultrafast Pulses Using Autocorrelation

Wahaj Ayub
23100023
LUMS School of Science and Engineering
(Dated: May 16, 2022)

In this experiment, we used the principle of an intensity auto-correlator to find the pulse width of an ultrafast femtosecond laser. The theoretical underpinnings of the process are defined in terms of optics and Maxwell's equations for a non linear dielectric material. The pulse width can then be used to find the peak power of the laser, which is important for use in applications. Additionally, we investigate the effects of adding a refractive material to the autocorrelator setup. It is shown that this changes the path length of one of the arms and causes a slight increase in the autocorrelation pulse width.

I. INTRODUCTION

Lasers were first experimentally realized in the 1950s and 1960s, when the first maser was built in 1953, while the first ruby laser was built in 1960 [1]. Since then, they have become inseparable from modern technology. Everything from DVD drives to optical communication makes the use of lasers. However, since then, many advances in laser technology have also been made. In particular, lasers with ultrashort wavelength pulses have been invented which can attain much higher peak power ranges than any continuous laser. These ultrafast lasers have numerous qualities that make them very suitable for applications such as spectroscopy and coherent control of atoms [2]. Additionally, they also find use in sensors, metrology and imaging [3].

To effectively utilize such a laser, we first need precise measurements of its features such as pulse width and peak power. However, often electronics fail to keep up with how fast these pulses are, giving rise to the need for more creative measurement techniques. How do you measure a process that is too fast to measure using anything else? Well, you measure it with itself. This is the basic principle behind autocorrelation [4]. Using this process, we can find the pulse width of the laser, as well as other properties such as peak power.

II. THEORETICAL BACKGROUND

In this section the basic background required to understand the operation of lasers that can emit femtosecond pulses will be described. Some familiarity with basic laser fundamentals will be assumed.

A. Pulsed Laser Operation and Mode Locking

Mode locking is a process through which ultrashort pulses can be obtained from continuous wave lasers [5]. This process is called mode locking as short pulses can be obtained by achieving a fixed phase relation between the different longitudinal mode inside the laser cavity. As

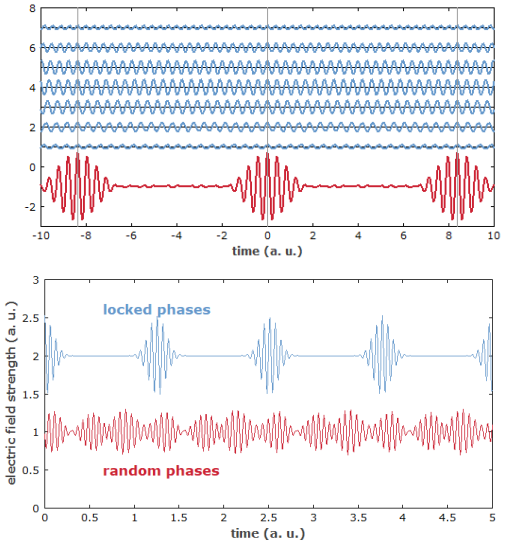

FIG. 1: Generation of pulses through mode-locking [5]

Fig. 1 shows, constructive and destructive interference between different modes can create short pulses of light. If we are able to fix these phase relations somehow, we have a mode-locked laser.

In this section, we will mostly focus on passive mode locking, in which a non linear passive element, like a saturable absorber, to achieve mode locking. An example of such a saturable absorber is a SESAM (or semiconductor saturable absorber mirror) [6]. In steady state, a saturable absorber works by absorbing any weaker unwanted pulses or background light, while only having only minimal losses for the main locked pulse. This is because the pulse saturates the absorber, reducing losses, which can then be made up through the laser gain [7]. A schematic for this process is shown in Fig. 2.

To get to the steady, for most passively locked lasers this can happen automatically, as the laser starts out in a continuous way, but fluctuations in the powers of different trips around the resonators causes the higher intensities to be favoured, resulting in the selection of single pulse, after many trips around the resonator. This is called self-start mode locking [7]. For some types of

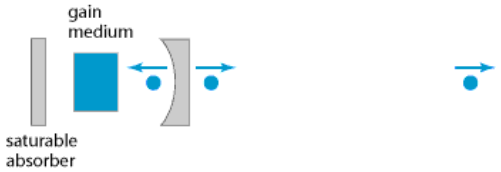

FIG. 2: Schematic of passive mode-locking [7]

passive mode locking, such as Kerr lens mode locking, this is not possible and they need to be started externally, for example by tapping the resonator mirror.

B. Nonlinear Optical Effects and Second Harmonic Generation

In most regimes, optical phenomena can be described in terms of linear effects, and parameters such as index of refraction and reflection coefficients. However, for high intensity light, as well as ultrafast pulses, this no longer suffices and non-linear effects play a major role. These effects can be characterized by considering the expansion of the polarization of a medium in terms of the electric field (in index notation)

$$\frac{P_i}{\epsilon_0} = \sum_j \chi^{(1)}_{ij} E_j + \sum_{jk} \chi^{(2)}_{ijk} E_j E_k + \sum_{jkl} \chi^{(3)}_{ijkl} E_j E_k E_l + \dots \quad (1)$$

where, for anisotropic materials, the susceptibility $\chi^{(n)}$ is an $(n+1)$-degree tensor [8]. Here the first order linear term describes linear optics, while the higher order terms account for non linear effects. In particular, we are interested in second order effects due to a non-zero $\chi^{(2)}$, which will lead to the phenomenon of second harmonic generation [9]. Due to symmetry considerations, this term can only be non-zero for a material that lacks inversion symmetry [3].

For the sake of mathematical simplicity we will assume that our electric field can be represented as

$$\mathbf{E} = \mathbf{A} e^{i(\mathbf{k}\cdot\mathbf{r}-\omega t)} + \mathbf{A}^* e^{-i(\mathbf{k}\cdot\mathbf{r}-\omega t)}. \quad (2)$$

We also assume that our electric field is polarized in the x direction. Thus we can write our second order polarization as

$$\begin{aligned} P^{(2)}_i &= \epsilon_0 \sum_{jk} \chi^{(2)}_{ijk} E_j E_k \\ &= \epsilon_0 \chi^{(2)}_{ixx} E_x^2 \\ &= \epsilon_0 \chi^{(2)}_{ixx} (A_x e^{i(\mathbf{k}\cdot\mathbf{r}-\omega t)} + A_x^* e^{-i(\mathbf{k}\cdot\mathbf{r}-\omega t)})^2 \\ &= \epsilon_0 \chi^{(2)}_{ixx} (2|A_x|^2 + A_x^2 e^{i(2\mathbf{k}\cdot\mathbf{r}-2\omega t)} + (A_x^*)^2 e^{-i(2\mathbf{k}\cdot\mathbf{r}-2\omega t)}). \end{aligned}$$

Notice that the first term is not time dependent and hence will not radiate, while the second and third term represent a polarization wave that is time dependent. For the rest of the working we will consider our crystal to be isotropic and take $\chi^{(2)}_{ixx} := \chi^{(2)}\delta_{ix}$. This gives us our final expression for the second order polarization:

$$\begin{aligned} \mathbf{P}^{(2)} &= 2|A_x|^2 \epsilon_0 \chi^{(2)} \hat{\mathbf{x}} \\ &+ \epsilon_0 \chi^{(2)} \left(A_x^2 e^{i(2\mathbf{k}\cdot\mathbf{r}-2\omega t)} + (A_x^*)^2 e^{-i(2\mathbf{k}\cdot\mathbf{r}-2\omega t)} \right) \hat{\mathbf{x}} \end{aligned} \quad (3)$$

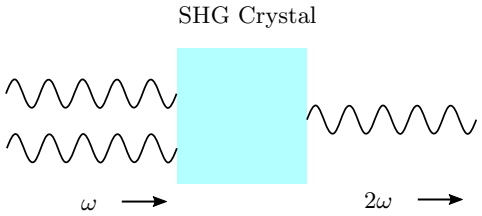

FIG. 3: Schematic of the second harmonic generation process

In a dispersionless, isotropic material, the Maxwell equations produce a driven wave equation that depends on the non linear part of the polarization

$$\nabla^2 \mathbf{E} - \frac{\epsilon}{c^2} \frac{\partial^2 \mathbf{E}}{\partial t^2} = \frac{1}{\epsilon_0 c^2} \frac{\partial^2 \mathbf{P}^{NL}}{\partial t^2}, \quad (4)$$

where the wave equation must hold for each frequency [8]. Through this, we can show that the time dependent polarization generates electromagnetic radiation with the frequency 2ω. This process is known as second harmonic generation. Fig. 3 represents the process in this diagram. We can use the wave equation and an ansatz to derive an expression for the intensity of the radiated wave, yielding

$$I_{\text{SHG}} = I^{\max}_{\text{SHG}} \left(\frac{\sin(\Delta k L/2)}{\Delta k L/2} \right)^2, \quad (5)$$

where $\Delta k = 2\mathbf{k} - \mathbf{k}_{\text{SHG}}$ [8]. Clearly, this intensity will be much greater if $\Delta k = 0$. This is known as the phase matching condition and ensures that our SHG beam travels in the same direction as our original seed beam.

C. Intensity Autocorrelation

The basics of second harmonic generation laid out in the previous section will aid in understanding autocorrelation. Given two identical parallel beams with a variable delay τ between them, it can be shown that by focusing both of them into a SHG crystal, "a signal light", at twice the frequency will be produced [4] such that

$$E_{\text{SHG}}(t,\tau) \propto E(t)E(t-\tau)$$

and hence

$$I_{\text{SHG}}(t,\tau) \propto I(t)I(t-\tau).$$

Since we have slow detectors, we can only measure the total intensity over a single pulse train, giving us our second order autocorrelation function

$$A^{(2)}(\tau) = \int_{-\infty}^{\infty} I(t)I(t-\tau). \tag{6}$$

This is a heuristic derivation of the second order intensity autocorrelation function, however, a rigorous and much more general derivation of interferometric autocorrelations can be found in Ref. [3]. The intensity autocorrelation function allows us to vary the delay τ and obtain a pulse width for the autocorrelation, which we can then use to find the pulse width of the original beam by multiplying an appropriate factor depending on the shape of the pulse. This is called the deconvolution factor κ. In addition to intensity autocorrelation, more complex methods such as FROG and interferometric autocorrelations can be used to find more information about the shape of the pulse.

Finding the width of the ultrafast laser pulse allows us to obtain important information about the laser. In particular, we are interested in it's peak power output. Using a slow detector we can only measure the average power P_{avg} over a certain period of time due to the laser. We can find the total energy of each pulse E_{pulse} by dividing the average power by the repetition rate R. Then to find the peak power output of the laser, we can just divide by the width (more precisely the full width at half maximum (FWHM)). In a more compact form,

$$P_{\text{peak}} = \frac{P_{\text{avg}}}{Rt_{\text{pulse}}}. \tag{7}$$

D. Effect of Refractive Material

In this section we will explain how adding a refractive material in the path of a femtosecond laser can affect its path, thus allowing us to calculate the refractive index of the material. Passing through such a material will slow the laser down and cause a time delay compared to the unaltered beam. The path delay due to travelling in a refractive material will be equal to

$$\Delta P_n = (n - n_0)d \tag{8}$$

where n_0 is the refractive index of air [10].

III. EXPERIMENTAL SETUP AND PROCEDURE

For all of the following experiments, the Avesta EFOA-SH, a fiber based femtosecond laser was used. This uses a fiber doped with Erbium (Er^{3+}) ions as the active gain medium. This laser uses passive mode locking to generate femtosecond pulses. The apparatus was set up according to Fig. 4, as shown in Fig. 5.

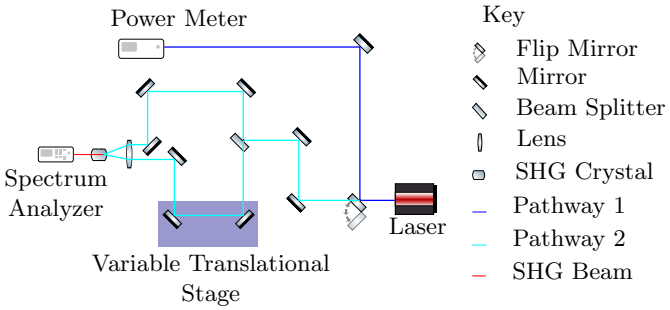

FIG. 4: Schematic diagram of the experimental setup [11]

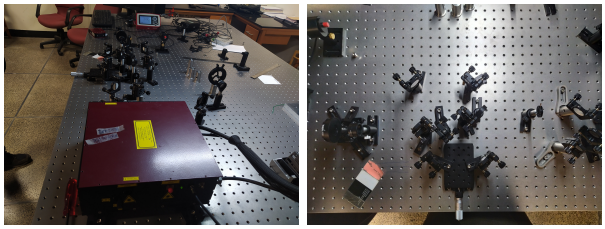

FIG. 5: Laboratory setup of the autocorrelator

Using the first path way, the power of the seed beam was measured using the Thorlabs PM100D digital power meter. Additionally, a wavelength spectrum of the seed beam was taken as well using the Thorlabs CCS200/M compact spectrometer and the Thorlabs OSA software. Then the optical pathway was switched by using the flip mirror. Additionally, a measurement for the repetition rate was made using an oscilloscope.

To generate the SHG beam, the femtosecond laser was passed through the second optical pathway, where it was split using a beam splitter, with one arm with a fixed length and one with a variable translation stage, with both arms combined at the end at a lens that focuses them on the Newlight BTC5050-SHG780(I)-P BBO crystal.

Then, an autocorrelation measurement was performed. The screw gauge dial on the translation stage was varied till we obtained a peak intensity on the spectrometer for the second harmonic beam. The spectrometer was calibrated so that there was no saturation in the spectrum for this intensity, and for further readings, it was ensured that the spectrometer remained calibrated. A wavelength spectrum was captured for this peak intensity. Then, the translational stage was adjusted slowly, with a spectrum being saved for every 0.05 mm on the translational stage. These data points were then collected and analysed further using python and Jupyter notebook.

After this, we aimed to determine the effect of introducing a slide of glass of 3.310 mm thickness in the path of the fixed arm of the interferometer. The autocorrelation measurement was performed again, repeating the steps outlined above. Additionally, the spectrum of the seed beam was again, due to there possibly being spec-

trum broadening due to thermal fluctuations before. By measuring the path delay due to the glass slide, and using Eq. (8), the refractive index of the glass slide was predicted. We also wished to investigate whether adding the glass slab would have any affect to the width of frequency spectrum of the SHG beam or the autocorrelation pulse width.

IV. RESULTS

As mentioned before, the data we obtained from the spectrometer was analyzed using a Jupyter notebook. The data was converted into '.txt' files and then imported directly into the software. Here, the wavelength spectra of the peak frequencies for both the SHG beam and seed beam were plotted. Additionally, an algorithm was used to find the Full Width at Half Maximum (FWHM) of the frequency spectra, which roughly correspond to the 'spectral width' of the light. The spectrum of the SHG beam can be found in Fig. 6. For the seed beam, two spectra were produced, once for the initial measurement, which had a broader spectrum (with an FWHM of 10.21 nm) possibly due unstable temperature of the laser, while the second one which more accurately corresponded to the results that had been obtained in the lab previously (with an FWHM of 9.37 nm) . These are shown in Fig. 7. The FWHM measured for the SHG beam was 2.37 nm without the glass slab in place.

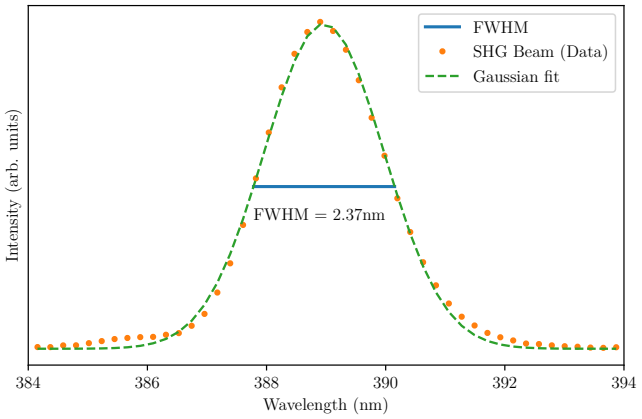

FIG. 6: The spectrum of the SHG beam

The data obtained for the repetition rate was also processed using python to produce Fig. 8, and to give the repetition rate of the pulses $R = 71.1$ MHz. The average power measured using the power meter for the laser was 32 mW.

To plot the autocorrelation, a peak finding algorithm was employed to find the maximum intensity for each τ, which was then plotted against τ to produce the autocorrelation of the pulse. We assumed that the pulses of our original beam were gaussian, and hence the autocorrelation was gaussian as well [12]. The plot obtained for the

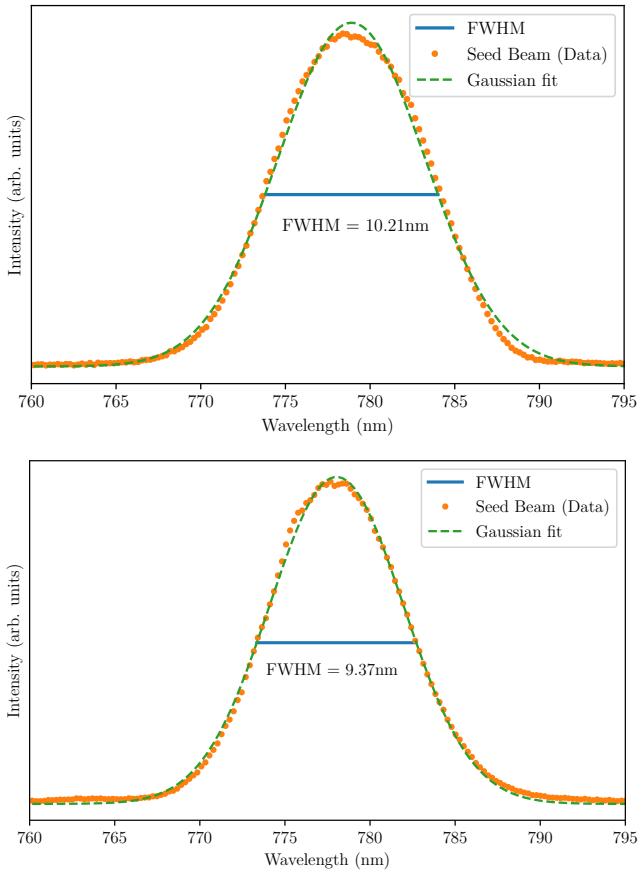

FIG. 7: The spectrum of the seed beam

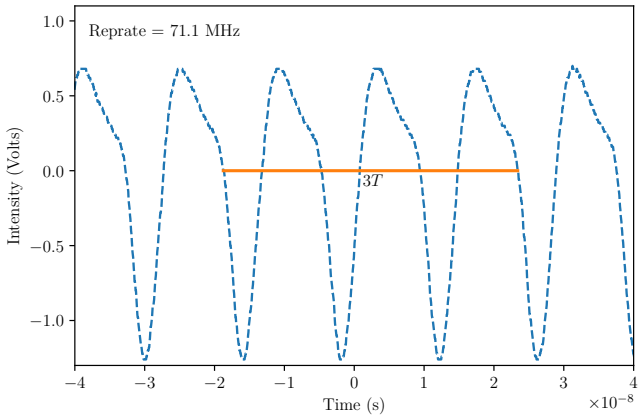

FIG. 8: Data from the oscilloscope

autocorrelation, as well as the FWHM is shown in Fig. 9. The pulse width for autocorrelation that we calculated was 75.1 fs, and using the deconvolution factor in Ref. [12], $\kappa = 1.414$, the pulse width of the original beam was calculated to be 53.11 fs. Then this was used to calculate the peak power of the femtosecond laser using Eq. (7). This was calculated to be equal to $P_{\text{peak}} = 8.474$ KW.

Next, the data for the autocorrelation with the glass

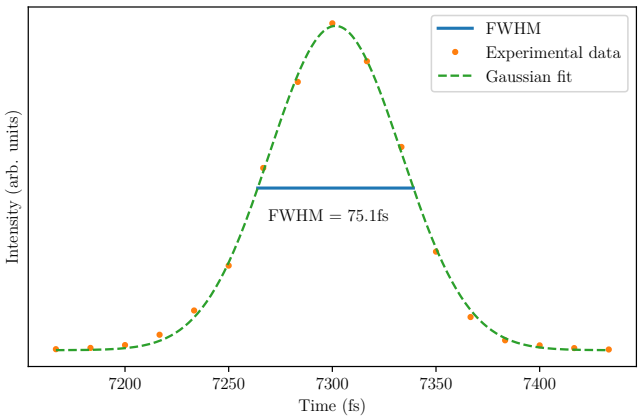

FIG. 9: Autocorrelation of the femtosecond pulse

slab placed was processed. As can be seen in Fig. 10, the width of the autocorrelation pulse appreciably increased to 79.70 fs. However, as seen in Fig. 11, the frequency spectrum has note changed much. Additionally, the maximum intensity (and hence the moment where $\tau = 0$) has changed when plotted along the translation stage distance. This allowed us to calculate the path difference between the laser with the slab and without the slab.

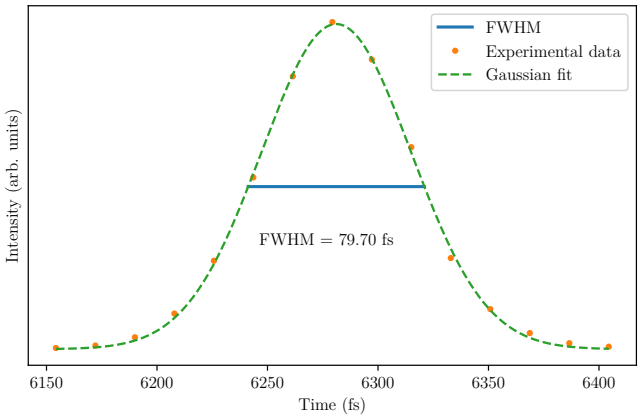

FIG. 10: Autocorrelation with glass slab in place

Using Eq. 8 and setting $n_0 = 1$ (which is a good approximation),

$$n = 1 + \frac{\Delta P_n}{d}, \tag{9}$$

where d is the thickness of the glass. Using the maximum intensity measurements, $\Delta P_n = (2.190 - 1.880)$ mm. Thus, the refractive index n was calculated to be 1.094. However, this value is far off from the accepted refractive index of glass and is an indication of a serious error within the experiment.

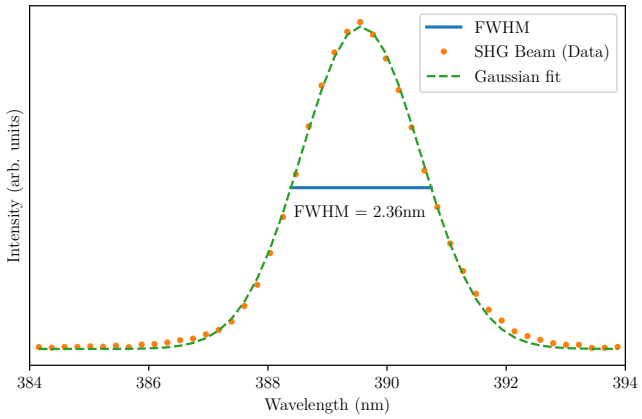

FIG. 11: SHG spectrum with glass slab in place

V. CONCLUSIONS

We demonstrated the working principle of an intensity autocorrelator and used it to measure the pulse width and peak power of the femtosecond laser. Overall, the process was made simpler through the use of automated data processing through python, and this can be used to simplify data processing for other experiments as well. The femtosecond laser has applications in many imaging and spectroscopy application [3], and hence measurements regarding important attributes such as peak power are essential. We also analyzed how the laser could be used to measure the refractive index of an unknown material, which has applications in biology [10].

However, there is significant room for improvement and further exploration. The width of seed beam and the pulse width were both different from those that had been measured in the laboratory previously. The refractive index was well off from the expected result as well. Further investigation is needed into why these results were off the mark and how we can obtain more reliable results from the set up. Additional techniques, such as FROG and interferometric autocorrelation, may be added to make the measurements more reliable and precise, as well as double checking the results.

[1] I. Kenyon, *The Light Fantastic: A Modern Introduction to Classical and Quantum Optics* (OUP Oxford, 2010).
[2] C. Rulliere, *Femtosecond Laser Pulses: Principles and Experiments*, Advanced Texts in Physics (Springer, 2005).
[3] J.-C. Diels and R. Wolfgang, *Ultrashort Laser Pulse Phenomena* (Academic Press, 2006).
[4] Intensity autocorrelation, `https://www.swampoptics.`

com/autocorrelation.html, accessed: 2022-04-12.

[5] R. Paschotta, article on 'mode locking' in the rp photonics encyclopedia, https://www.rp-photonics.com/mode_locking.html (2022), accessed: 2022-04-16.

[6] U. Keller, K. Weingarten, F. Kartner, D. Kopf, B. Braun, I. Jung, R. Fluck, C. Honninger, N. Matuschek, and J. Aus der Au, Semiconductor saturable absorber mirrors (sesam's) for femtosecond to nanosecond pulse generation in solid-state lasers, IEEE Journal of Selected Topics in Quantum Electronics **2**, 435 (1996).

[7] R. Paschotta, article on 'passive mode locking' in the rp photonics encyclopedia, https://www.rp-photonics.com/passive_mode_locking.html (2022), accessed: 2022-04-16.

[8] R. W. Boyd, *Nonlinear Optics (Fourth Edition)* (Academic Press, 2020).

[9] R. Paschotta, article on 'autocorrelators' in the rp photonics encyclopedia, https://www.rp-photonics.com/autocorrelators.html (2022), accessed: 2022-04-12.

[10] B. Hussain, M. Nawaz, M. Ahmed, and M. Y. A. Raja, Measurement of thickness and refractive index using femtosecond and terahertz pulses, Laser Physics Letters **10**, 055301 (2013).

[11] A. Franzen, Componentlibrary, http://www.gwoptics.org/ComponentLibrary/, accessed: 2022-04-12.

[12] S. A. Aljunid, Optical autocorrelation using non-linearity in a simple photodiode (2007).